Design and implementation of grid multi-scroll fractional-order chaotic attractor

Liping Chen,Wei Pan, Ranchao Wu, J. A. Tenreiro Machado, and António M. Lopes

This paper proposes a novel approach for generating multi-scroll chaotic attractors in multi-directions for fractional-order (FO) systems. The stair nonlinear function series and the saturated nonlinear function are combined to extend equilibrium points with index 2 in a new FO linear system. With the help of stability theory of FO systems, stability of its equilibrium points is analyzed, and the chaotic behaviors are validated through phase portraits, Lyapunov exponents, and Poincaré section. Choosing the order 0.96 as an example, a circuit for generating 2-D grid multiscroll chaotic attractors is designed, and 2-D 9×9 grid FO attractors are observed at most. Numerical simulations and circuit experimental results show that the method is feasible and the designed circuit is correct.

With the development of fractional-order (FO) calculus, it is well verified that many nonlinear FO differential systems, such as the FO Duffing oscillator, the FO Chua circuit, or the so-called FO Rössler, FO Chen, FO Lorenz, and FO Lü systems, among others, exhibit complex bifurcations and chaotic phenomena. These systems can generate single-scroll or double-scroll chaotic attractors. Multi-scroll chaotic attractors (MSCA) admit much more complex dynamic behaviors, more adjustability, and more encryption parameters. Therefore, MSCA have more potential application to communications, cryptography, and many other fields. Naturally, the design and implementation of fractional MSCA is an interesting and challenging topic. In this paper, a new MSCA generation method will be introduced, which is different from the existing ones. In addition, circuit experimental results of the generation of fractional MSCA are presented.

I. INTRODUCTION

The study of chaos started about 300 years ago and the discovery of the Lorenz system brought the area into a new era. Since chaos is useful in many fields, such as secure communication, signal processing, digital data, systems identification, data encryption, nonlinear optimization, power systems, and others,[1–3] generating chaos has received attention from many scholars.

Compared with the single-scroll chaotic attractors, it is well known that MSCA reveal much more complex topological structures and dynamic behaviors. They have been used in secure communications and encryption. Therefore, the generation of MSCA is a subject of increasing interest, and a considerable number of researchers have done work in this field.[4–13] For example, Tang *et al*. introduced a sine-function approach to generate n-scroll attractors, and a 9-scroll-attractor was observed for the first time.[4,5] Later, Yalcin *et al*. presented a family of multi-directional, MSCA by adopting a stair nonlinear function series (SNFS) method, including 1-D n-scroll, 2-D $n \times m$-scroll, and 3-D $n \times m \times p$-scroll attractors.[6] Lü *et al*. presented a hysteresis to generate 1-D, 2-D, and 3-D multi-directional MSCA.[7–11] Soon afterwards, Lü *et al*. proposed a saturated nonlinear function (SNLF) approach to create 1-D, 2-D, and 3-D multi-directional MSCA.[12] Zhang and Yu introduced two different kinds of piecewise-linear functions (PWLF) to generate multi-directional MSCA in a single system.[13] Nowadays, there are many methods to design and realize MSCA in the classical differential systems.[14–16]

In the last decades, fractional calculus have gained considerable research attention for its more advantages than classical integer-order ones in describing memory and hereditary properties of many materials and processes.[17–23] It was recognized that many fractional-order (FO) nonlinear differential systems, including the FO Duffing oscillator,[24] the FO Chua circuit,[25] or the so-called FO Rössler,[26] FO Chen,[27] FO Lorenz,[28] FO Lü,[29] and FO Liu systems,[30] exhibit complex bifurcations and chaotic phenomena. Moreover, the research on the multi-directional MSCA generated from FO linear autonomous systems by adding different functions has also been reported. In fact, topological structures of MSCA in FO systems are different from those in the classical differential systems because of the nonlocal properties of FO differential operators. Only a few FO systems capable of generating multi-directional MSCA have been reported in recent years. For instance, Deng *et al*. proposed the SNFS, the SNLF, and the hysteresis series methods to generated multi-directional MSCA based on a specific FO differential linear system.[31–33] Sun *et al*. discussed the generation of MSCA based on the

switched FO multi-model systems.[35] Ahmad[36] demonstrated that multiple-scroll attractors can be obtained from FO chaotic systems by using a modified nonlinearity and an appropriate set of control parameters. Xu[37] investigated the generation of multi-wing chaotic attractors using integer and FO linear differential equation systems with switching controls.

Note that one kind of PWLF was used to generate multi-directional MSCA in the above papers. No one has tried to create multi-directional MSCA in one single FO system employing two (or more) different kinds of PWLF. Therefore, it is interesting to ask whether the FO system can also generate multi-directional MSCA, by using two different kinds of PWLF, such as the SNFS and the SNLF, It is worth mentioning that the SNFS and the SNLF are different kinds of functions which have different forming mechanisms. Our work gives a positive answer to the question formulated above. Moreover, it should be pointed out that these aforementioned MSCA, created from FO systems, were only verified by numerical simulations.[31–33,35–37] To the best of our knowledge, there are few results about circuit realization of MSCA generated from FO systems. Nonetheless, it is more substantive to implement the FO system by circuits than merely by simulating them.

Motivated by the above discussions, this paper proposes a novel FO system with multi-directional MSCA, which is not topological equivalent to the systems in References 31–33 and 35–37. Similarly, the equilibrium points with index 2 of this system can be extended by adding breakpoints into the PWLF. Two different PWLF, SNFS and SNLF, are combined to generate MSCA in our FO system in the x-y or the y-x planes. That is to say, we use SNFS to generate attractors in x-axis and SNLF in y-axis, or SNFS in y-axis and SNLF in x-axis. It is straightforward to see that the attractors generated by two different kinds of functions are topologically nonequivalent to those generated by only one kind of function. The dynamical behavior of the multi-directional multi-scroll system is further investigated by employing phase portraits, the Lyapunov exponents, and Poincaré section. A simple circuit of order 0.96 is designed, and as many as 9×9 attractors are observed.

The rest of this paper is organized as follows. In Section II, some preliminaries of the FO system are presented. In Section III, the generation of FO multi-directional MSCA is considered. In Section IV, a circuit is designed, and several experimental results are presented. Finally, in Section V, conclusions are drawn.

II. PRELIMINARIES

This section briefly introduces several basic definitions of the fractional calculus.

There are many different kinds of definitions for FO derivatives, but the most commonly used ones are the Riemann-Liouville and the Caputo definitions.

Definition 1. (Podlubny[19]) The FO integral (Riemann-Liouville integral) $D_{t_0,t}^{-\alpha}$ with FO $\alpha \in R^+$ of function $x(t)$ is defined as

$$D_{t_0,t}^{-\alpha}x(t) = \frac{1}{\Gamma(\alpha)}\int_{t_0}^{t}(t-\tau)^{\alpha-1}x(\tau)d\tau,$$

where $\Gamma(\cdot)$ is the gamma function, $\Gamma(\tau) = \int_0^\infty t^{\tau-1}e^{-t}dt$.

Definition 2. (Podlubny[19]) The Riemann-Liouville derivative of FO α of function $x(t)$ is given as

$$\begin{aligned} {}_{RL}D_{t_0,t}^{\alpha}x(t) &= \frac{d^n}{dt^n}D_{t_0,t}^{-(n-\alpha)}x(t), \\ &= \frac{d^n}{dt^n}\frac{1}{\Gamma(n-\alpha)}\int_{t_0}^{t}(t-\tau)^{n-\alpha-1}x(\tau)d\tau, \end{aligned}$$

where $n-1 < \alpha < n \in Z^+$.

Definition 3. (Podlubny[19]) The Caputo derivative of FO α of function $x(t)$ is defined as

$$\begin{aligned} {}_{C}D_{t_0,t}^{\alpha}x(t) &= D_{t_0,t}^{-(n-\alpha)}\frac{d^n}{dt^n}x(t), \\ &= \frac{1}{\Gamma(n-\alpha)}\int_{t_0}^{t}(t-\tau)^{n-\alpha-1}x^{(n)}(\tau)d\tau, \end{aligned}$$

where $n-1 < \alpha < n \in Z^+$.

In this paper, we adopt the Caputo FO derivative, D^α, because of its convenience in engineering applications.

The stability of FO systems is different from that in the integer case. So, the following definitions and lemmas are presented firstly.

Definition 4. (Deng and Lü[33]) Considering a general n-dimensional FO system

$$D^\alpha(X) = f(X) \tag{1}$$

the roots of the equation $f(X) = 0$ are called the equilibrium points of the system, where $D^\alpha(X) = (D^\alpha x_1, D^\alpha x_2, ..., D^\alpha x_n)^T$, $X = (x_1, x_2, ..., x_n)^T \in R^n$.

Definition 5. (Li and Ma[38]) Suppose that E is an equilibrium point of system (1), and that all the eigenvalues $\lambda_i(J)$ $(i = 1, 2, \ldots, n)$ of the Jacobi matrix J at the equilibrium point E satisfy: $|\lambda_i(J)| \neq 0$ and $|arg(\lambda_i(J))| \neq \alpha\pi/2$, then we call E a hyperbolic equilibrium point. The symbol J denotes the Jacobi matrix of $f(X) = 0$, and λ_i are the eigenvalues of J.

It follows from the Theorem 3 proposed in Ref. 38 that the vector field $f(x)$ is topologically equivalent with its linearization vector field Jx in the neighborhood of the equilibrium point E if E is a hyperbolic equilibrium point. Therefore, the following lemma (Lemma 1) can serve as an effective way to determine the stability of system (1) at E.

Lemma 1. (Deng and Lü[33]) For $n = 3$, system (1) is asymptotically stable at the equilibrium points, E, if $|arg(\lambda_i(J))| > \alpha\pi/2$, $i = 1, 2, 3$.

Lemma 2. (Cafagna and Grass[34]) The equilibrium point, E, of system (1) is unstable if the order α satisfies the condition below for at least one eigenvalue

$$\alpha > \frac{2}{\pi} arc\tan\frac{|Im(\lambda)|}{|Re(\lambda)|}.$$

Lemma 3. (Deng and Lü[33]) For $n = 3$, if one of the eigenvalues is $\lambda_1 < 0$ and the other two conjugate eigenvalues $|arg(\lambda_2)| = |arg(\lambda_3)| < \alpha\pi/2$, then the equilibrium

point, E, is called a saddle point with index 2; if one of the eigenvalues $\lambda_1 > 0$ and the other two conjugate eigenvalues are $|arg(\lambda_2)| = |arg(\lambda_3)| > \alpha\pi/2$, then the equilibrium point, E, is called a saddle point with index 1.

A chaotic attractor is generally considered to be generated around saddle points with index 2. One saddle point with index 2 will generate one attractor at most.

III. GENERATING MULTI-DIRECTIONAL MULTI-SCROLL ATTRACTORS

A. Model and numerical simulations

We introduce here a simple 3-dimensional autonomous FO system

$$\begin{cases} D^\alpha x = y + z, \\ D^\alpha y = \mu z, \\ D^\alpha z = -x - z, \end{cases} \tag{2}$$

where μ is constant, $\mu > 0$, and α is system order, $0 < \alpha < 1$. System (2) has only one equilibrium point (0, 0, 0). The characteristic equation of (2) at equilibrium (0, 0, 0) is given by

$$\lambda^3 + \lambda^2 + \lambda + \mu = 0. \tag{3}$$

Denoting $\Delta = \mu - 2/27$ and $\delta = \mu^2/4 - (7/54)\mu - 1/36$, then the roots of Equation (2) are as follows:

$$\lambda_1 = -\frac{1}{3} + \sqrt[3]{-\frac{\Delta}{2} + \sqrt{\delta}} + \sqrt[3]{-\frac{\Delta}{2} - \sqrt{\delta}}$$

and

$$\begin{aligned} \lambda_{2,3} &= -\frac{1}{3} - \frac{1}{2}\left(\sqrt[3]{-\frac{\Delta}{2} + \sqrt{\delta}} + \sqrt[3]{-\frac{\Delta}{2} - \sqrt{\delta}}\right) \\ &\quad \pm \frac{\sqrt{3}}{2} i \left(\sqrt[3]{-\frac{\Delta}{2} + \sqrt{\delta}} - \sqrt[3]{-\frac{\Delta}{2} - \sqrt{\delta}}\right), \\ &= \beta \pm \gamma i, \end{aligned}$$

where $\beta = Re(\lambda_{2,3})$, $\gamma = |Im(\lambda_{2,3})|$. The stability of the equilibrium point (0, 0, 0) of system (2) is determined by Lemmas 1 and 2. According to Lemma 3, (0, 0, 0) is a saddle point with index 2 if $\lambda_1 < 0$, $\beta > 0$, $\gamma \neq 0$ and $|\arctan(\gamma/\beta)| < \alpha\pi/2$. Hereafter, one always chooses a suitable μ to ensure that the characteristic equation of a certain equilibrium of the system has one negative real root λ_1 and a pair of conjugate complex roots $\lambda_{2,3} = \beta \pm \gamma i$, where $\beta > 0, \gamma \neq 0$, $|\arctan(\gamma/\beta)| < \alpha\pi/2$.

Since (2) is linear, for this system to be chaotic, we need to bring nonlinear terms into it. We know that one saddle point with index 2 will only generate one attractor at most. The generation of multi-directional MSCA will need a large number of saddle points with index 2, so the main idea is to add breakpoints into nonlinear functions in system (2). To this end, the system (2) is recasted as follows:

$$\begin{cases} D^\alpha x = y + z - f(y), \\ D^\alpha y = \mu z, \\ D^\alpha z = -x - z + f(x), \end{cases} \tag{4}$$

where $0 < \alpha < 1$ is order and $\mu > 0$. Functions $f(x)$ and $f(y)$ are PWLF. By choosing suitable PWLF and μ, system (4) can generate multi-directional MSCA.

To generate multi-directional MSCA, two different kinds of PWLF, namely, the SNFS and the SNLF, are chosen and added to system (2) to show the working principle. Take

$$\begin{aligned} F_1(x) = \sum_{k=-K, k\neq 0}^{k=K} \frac{p}{2q} \Bigg\{ &\left| x - p\left(2k - \frac{|k|}{k}\right) + q \right| \\ &- \left| x - p\left(2k - \frac{|k|}{k}\right) - q \right| \Bigg\}, \end{aligned}$$

and

$$\begin{aligned} F_2(x) = A_1 sgn(x) &+ \sum_{n=1}^{N} sgn(x - 2nA_2) \\ &+ \sum_{m=1}^{M} sgn(x + 2mA_3), \end{aligned}$$

where K, M, N, m, n are positive integers, k is an integer, $A_1, A_2, A_3, p > 0$, and $q \in (0, p)$. Note that $F_1(x)$ is a SNLF, the saturated slope is p/q, and the delay time is $(2k - |k|/k)p$. Function $F_2(x)$ is a SNFS. System (4) can generate $(2K + 1)$ attractors in x-axis or y-axis when $f(x) = F_1(x)$ or $f(y) = F_1(x)$, respectively. Similarly, $(m + n + 1)$ attractors will be created in system (4) by F_2 in x-axis or y-axis when $A_1 = 0$, and $(n + m + 2)$ attractors will be generated when $A_1 \neq 0$. The parameters K, p, q, A_1, A_2, A_3 are all adjustable. By changing these parameters, one can design the number of the equilibrium points as necessary conditions to generate MSCA.

Let $p = 1, q = 0.02p, K = 2, A_1 = A_2 = A_3 = 1, m = n = 1$, thus forming 5×4 attractors in x-y plane, corresponding to the type 1 attractors in Table I. The attractors in x-axis are generated by SNLF and y-axis by SNFS. Since SNFS and SNLF are different kinds of functions, which have different forming mechanisms. Topologies of attractors created by different combinations of those are not equivalent with each other. Table I gives the details of some parameters and the corresponding multi-directional MSCA generated with these parameters, where Type 1, 2, 3, and 4 in Table I are used to identify these different attractors. That is to say, Type 1, 2, 3, and 4 attractors are created by the combinations of SNLF and SNFS, SNLF and SNLF, SNFS and SNLF, SNFS and SNFS, respectively. Take the parameters $p = 1$, $q = 0.02p$ in Table I. Numerical simulations are depicted in Figs. 1(a)–1(d). The parameters in Table I are not unique and can be chosen within a certain range while the system still keeps chaotic.

TABLE I. Attractors generated with parameters $\mu, K, M, N, A_1, A_2, A_3$.

Type	x-axis	y-axis	μ	K	M	N	A_1	A_2	A_3	A	Attractors
1	SNLF	SNFS	2.5	2	1	1	1	1	1	0.96	5×4
2	SNLF	SNLF	2.5	2	…	…	…	…	…	0.96	5×5
3	SNFS	SNLF	3	2	1	1	0	0.5	0.5	0.9	3×5
4	SNFS	SNFS	2.5	…	2	2	1	1	1	0.96	6×6

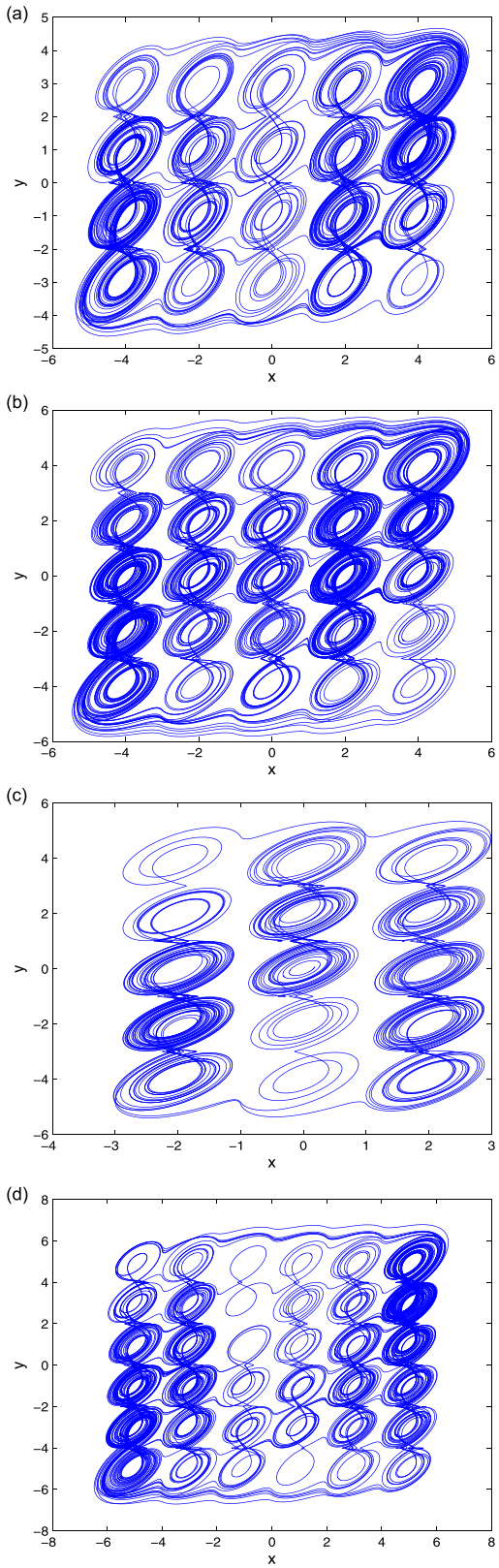

FIG. 1. Phase portrait of four kinds of attractors: (a) type 1; (b) type 2; (c) type 3; (d) type 4.

The distribution of the locations of all four kinds of attractors is listed in Tables II–V.

Remark 1. In fact, by using only one kind of PWLF, SNFS or SNLF, one-directional MSCA in x-axis or y-axis can be generated in the system.

TABLE II. Location of attractors of type 1 attractors.

$(-4, 3, 0)$	$(-2, 3, 0)$	$(0, 3, 0)$	$(2, 3, 0)$	$(4, 3, 0)$
$(-4, 1, 0)$	$(-2, 1, 0)$	$(0, 1, 0)$	$(2, 1, 0)$	$(4, 1, 0)$
$(-4, -1, 0)$	$(-2, -1, 0)$	$(0, -1, 0)$	$(2, -1, 0)$	$(4, -1, 0)$
$(-4, -5, 0)$	$(-2, -3, 0)$	$(0, -3, 0)$	$(2, -3, 0)$	$(4, -3, 0)$

TABLE III. Location of attractors of type 2 attractors.

$(-4, 4, 0)$	$(-2, 4, 0)$	$(0, 4, 0)$	$(2, 4, 0)$	$(4, 4, 0)$
$(-4, 2, 0)$	$(-2, 2, 0)$	$(0, 2, 0)$	$(2, 2, 0)$	$(4, 2, 0)$
$(-4, 0, 0)$	$(-2, 0, 0)$	$(0, 0, 0)$	$(2, 0, 0)$	$(4, 0, 0)$
$(-4, -2, 0)$	$(-2, -2, 0)$	$(0, -2, 0)$	$(2, -2, 0)$	$(4, -2, 0)$
$(-4, -4, 0)$	$(-2, -4, 0)$	$(0, -4, 0)$	$(2, -4, 0)$	$(4, -4, 0)$

TABLE IV. Location of attractors of type 3 attractors.

$(-2, 4, 0)$	$(0, 4, 0)$	$(2, 4, 0)$
$(-2, 2, 0)$	$(0, 2, 0)$	$(2, 2, 0)$
$(-2, 0, 0)$	$(0, 0, 0)$	$(2, 0, 0)$
$(-2, -2, 0)$	$(0, -2, 0)$	$(2, -2, 0)$
$(-2, -4, 0)$	$(0, -4, 0)$	$(2, -4, 0)$

TABLE V. Location of attractors of type 4 attractors.

$(-5, 5, 0)$	$(-3, 5, 0)$	$(-1, 5, 0)$	$(1, 5, 0)$	$(3, 5, 0)$	$(5, 5, 0)$
$(-5, 3, 0)$	$(-3, 3, 0)$	$(-1, 3, 0)$	$(1, 3, 0)$	$(3, 3, 0)$	$(5, 3, 0)$
$(-5, 1, 0)$	$(-3, 1, 0)$	$(-1, 1, 0)$	$(1, 1, 0)$	$(3, 1, 0)$	$(5, 1, 0)$
$(-5, -1, 0)$	$(-3, -1, 0)$	$(-1, -1, 0)$	$(1, -1, 0)$	$(3, -1, 0)$	$(5, -1, 0)$
$(-5, -3, 0)$	$(-3, -3, 0)$	$(-1, -3, 0)$	$(1, -3, 0)$	$(3, -3, 0)$	$(5, -3, 0)$
$(-5, -5, 0)$	$(-3, -5, 0)$	$(-1, -5, 0)$	$(1, -5, 0)$	$(3, -5, 0)$	$(5, -5, 0)$

Remark 2. From Figs. 1(a)–1(d), we can easily verify the difference between the four kinds of attractors.

B. Dynamic behavior analysis

In this section, take the type 2 MSCA as an example to analyze dynamic behavior. The corresponding system of type 2 attractors is

$$\begin{cases} D^{\alpha}x = y + z - F_1(y), \\ D^{\alpha}y = \mu z, \\ D^{\alpha}z = -x - z + F_1(x). \end{cases} \tag{5}$$

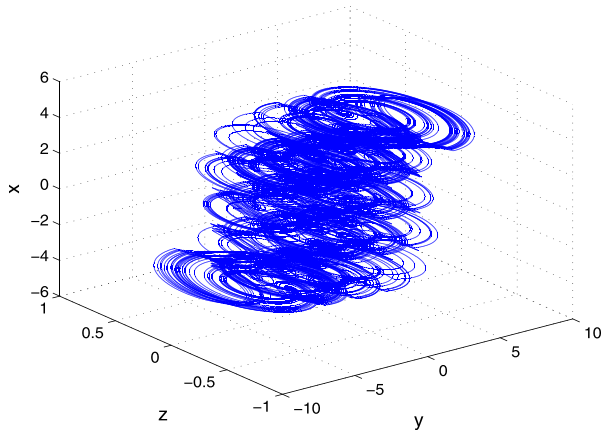

FIG. 2. The 3-D phase portrait of type 2 attractors.

According to Table I, one has the parameters $\mu = 2.5$, $K = 2$, $p = 1$, $q = 0.02p$, and $\alpha = 0.96$. Fig. 2 shows the 3-D phase portrait of 5×5 attractors of type 2. Fig. 3(a) shows the largest Lyapunov exponent with respect to μ of system (5), Fig. 3(b) represents the Poincaré map on section $y = 0$, and Fig. 3(c) shows the largest Lyapunov exponent with respect to α of system (5). Making $D^\alpha x = D^\alpha y = D^\alpha z = 0$, yields $y - F_1(y) = 0$, $z = 0$, and $-x + F_1(x) = 0$. All the equilibrium points of system (5) are calculated and depicted in Fig. 4. We verify that there are $(2k+1) \times (2K+1) + 2K \times 2K = 41$ equilibrium points.

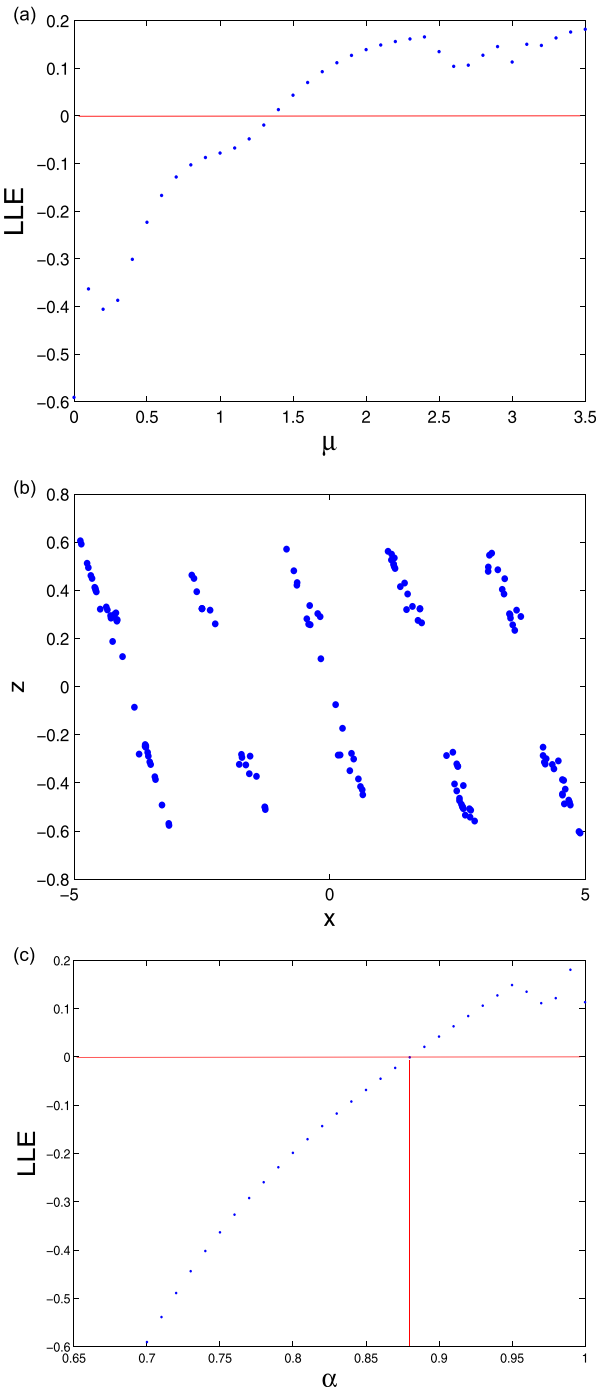

FIG. 3. (a): Largest Lyapunov exponent of system (5) with respect to μ. (b): Poincaré map of system (5) on section $y = 0$. (c): Largest Lyapunov exponent of system (5) with respect to α.

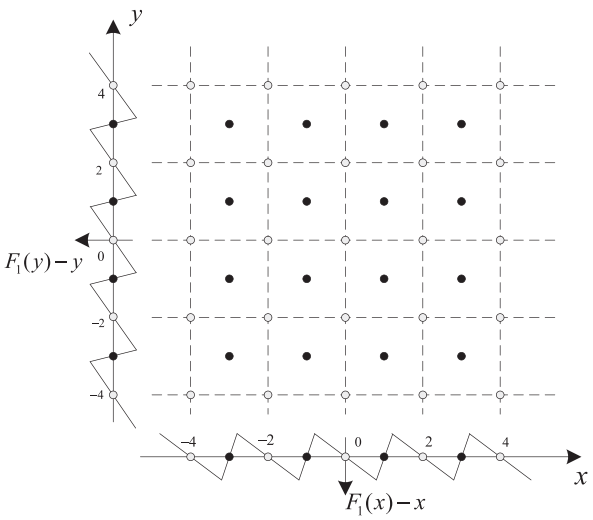

FIG. 4. Equilibrium point distribution of system (5).

At equilibrium point $E^* = (x^*, y^*, z^*)$, the Jacobi matrix of system (5) is

$$J_{E^*} = \begin{pmatrix} 0 & 1 - F_1'(y^*) & 0 \\ 0 & 0 & \mu \\ F_1'(x^*) - 1 & 0 & -1 \end{pmatrix}, \tag{6}$$

where $F_1'(y^*) = \frac{dF_1(y)}{dy}|_{y^*}$, $F_1'(x^*) = \frac{dF_1(x)}{dx}|_{x^*}$.

The derivative of $F_1(u)$ at point u^*(u denotes x or y) is

$$\begin{aligned} F_1'(u^*) &= \left.\frac{dF_1(u)}{du}\right|_{u^*}, \\ &= \sum_{k=-K, k\neq 0}^{k=K} \frac{p}{2q} \left\{ sgn\left(u^* - p\left(2k - \frac{|k|}{k}\right) + q\right) \right. \\ &\quad \left. - sgn\left(u^* - p\left(2k - \frac{|k|}{k}\right) - q\right) \right\}. \end{aligned}$$

If $u^* = 2kp$, $k = 0, \pm 1, \pm 2, \ldots \pm K$, which corresponds to the equilibrium points marked as '$\circ$' in Fig. 4, then $F_1'(u^*) = 0$. Alternatively, if $u^* = (2k - |k|/k)p$, $k = 0, \pm 1, \pm 2, \ldots \pm K$, which correspond to the equilibrium points marked as '$\bullet$' in Fig. 4, then $F_1'(u^*) = p/q$.

The characteristic equation of matrix (6) is

$$\begin{aligned} f(\lambda) = \lambda^3 + \lambda^2 - (F_1'(x^*) - 1)\lambda \\ + \mu(F_1'(x^*) - 1)(F_1'(y^*) - 1) = 0. \end{aligned} \tag{7}$$

For equilibrium points '$\circ$', as $F_1'(x^*) = F_1'(y^*) = 0$, then the characteristic equation can be simplified to

$$f(\lambda) = \lambda^3 + \lambda^2 + \lambda + \mu = 0. \tag{8}$$

The roots of Equation (8) are $\lambda_1 = -1.4732$, $\lambda_{2,3} = 0.2366 \pm 1.2810i$, yielding $|arg(\lambda_{2,3})| = 1.3882 < 1.5080 = \alpha\pi/2$. According to Lemma 3, points '$\circ$' are saddle points with index 2, and an attractor will form around each '$\circ$'. For equilibrium points '$\bullet$', $F_1'(x^*) = F_1'(y^*) = p/q = 50$ and the characteristic equation can be simplified to

$$f(\lambda) = \lambda^3 + \lambda^2 + (1 - p/q)\lambda + (1 - p/q)^2\mu = 0. \quad (9)$$

The roots of Equation (9) are $\lambda_1 = -19.4269, \lambda_{2,3} = 9.2135 \pm 14.9697i$, yielding $|arg(\lambda_{2,3})| = 1.0191 < 1.5080 = \alpha\pi/2$. According to Lemma 3, points '•' are saddle points with index 2. However, numerical simulation in Fig. 1(d) shows that only points '○' can generate attractors. In fact, having a saddle point with index 2 is only a necessary condition, not a sufficient one for generating attractors. According to the Homoclinic Ŝilnikov Theorem,[39] it is needed a condition-existence of a homoclinic orbit in the neighboring region of the equilibrium point to generate attractors. This is the reason why we say, that one saddle point with index 2 will generate only one attractor at most.

The attractors of type 1, type 3, and type 4 can be investigated in the same way.

IV. CIRCUIT IMPLEMENTATION FOR MULTI-SCROLL ATTRACTORS

In this section, several circuit diagrams are designed to realize various MSCA. Circuit implementation is somewhat different from numerical simulation due to hardware limitations. Since circuits cannot keep such a high operational precision as computers, some distortion will be introduced and the input signal cannot be well tracked under the condition of large input signals. We know that chaotic systems are very sensitive to the initial values and the parameters of the system. Therefore, it is difficult to control the value of the resistors and the capacitors very precisely in the circuit implementation.

In a FO circuit, since there is not a device to implement directly the FO calculations, we adopt a number of resistors and capacitors connecting in parallel, or in series, to approximate the transfer function of $1/s^{\alpha}$ (where α is the order), which often causes an increasing error. Up to now, there are no results reported in the literature about generation of FO multi-directional multi-scroll using a circuit.

Firstly, we investigate the circuit diagram which is the basic cell for designing the SNLF in Fig. 5(a). The operational amplifier in Fig. 5(a) is the TL082. Moreover, all original devices in our circuit diagrams below are operational amplifiers of type TL082 with voltage supply ± 15 V and saturated output voltage about ± 13.5 V.

The U_i–U_o relationship of the ith basic cell, depicted in Fig. 5(b), is given by

$$U_o = \begin{cases} V_{sat} & if \quad U_i < \left(E_i - V_{sat}\dfrac{R_2}{R_1}\right), \\ -\dfrac{R_1}{R_2}(U_i - E_i) & if \quad \left(E_i - V_{sat}\dfrac{R_2}{R_1}\right) \le U_i \le \left(E_i + V_{sat}\dfrac{R_2}{R_1}\right), \\ -V_{sat} & if \quad U_i > \left(E_i + V_{sat}\dfrac{R_2}{R_1}\right), \end{cases} \quad (10)$$

where U_i and U_o are the input and the output voltages (notice that the subscript i of U_i means 'input', not ith). Furthermore,

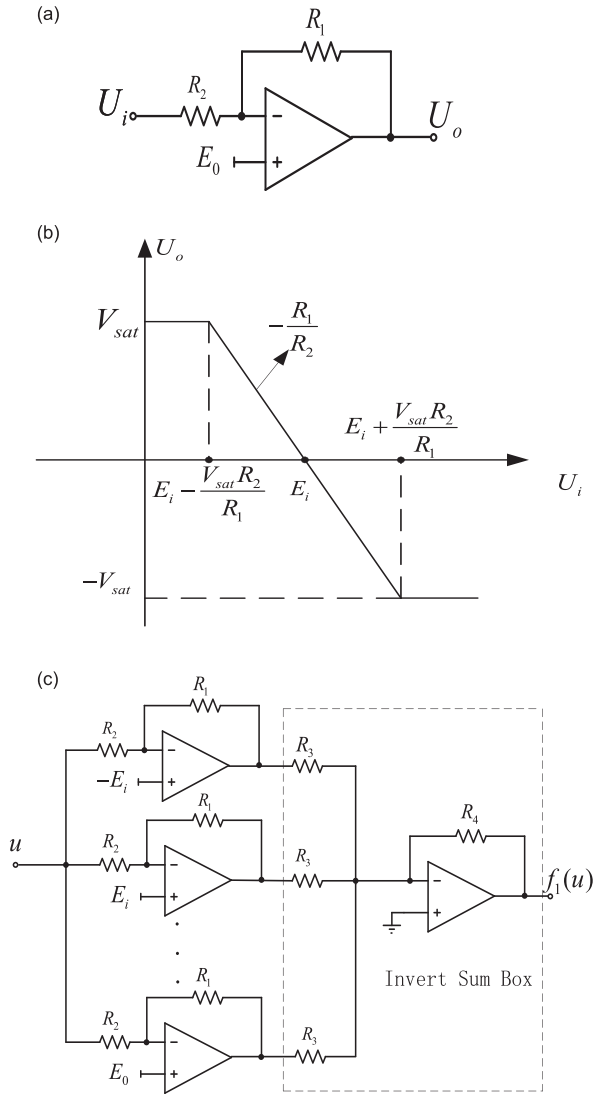

FIG. 5. The circuit diagram. (a) basic cell, (b) U_i–U_o relationship, and (c) the realization of $f_1(u)$.

V_{sat} denotes the saturated output voltage of the operational amplifier so that $V_{sat} = 13.5$ V. The values $(E_i - V_{sat}R_2/R_1)$ and $(E_i + V_{sat}R_2/R_1)$ are switching points of the ith cell, and the slope is $-R_1/R_2$. Equation (10) can be rewritten as

$$U_o = -\frac{R_1}{2R_2}\left\{\left|U_i - E_i + \frac{V_{sat}R_2}{R_1}\right| - \left|U_i - E_i - \frac{V_{sat}R_2}{R_1}\right|\right\}.$$

By connecting several basic cells in parallel, and adding an invert sum box circuit in series, as shown in Fig. 5(c), we can easily deduce that

$$f_1(u) = \sum_{k=-K, k\neq 0}^{k=K} \frac{R_1R_4}{2R_2R_3}\left\{\left|u - E_i + \frac{V_{sat}R_2}{R_1}\right| - \left|u - E_i - \frac{V_{sat}R_2}{R_1}\right|\right\}. \quad (11)$$

Let us assume that $E = 1$ is the unit voltage and take $E_i = (2k - |k|/k)E$. Comparing Equation (11) with function $F_1(x)$, we obtain that $q = V_{sat}R_2/R_1$ and $p = E$. If we set

$R_1 = 200$ kΩ, since $q = 0.02$ and $V_{sat} = 13.5$ V, then $R_2 = 300\,\Omega$. While $R_1R_4/2R_2R_3 = p/2q$, we set $R_4 = 1$ kΩ, and then $R_3 = 13.5$ kΩ. Thus, Equation (10) can be perfectly realized using a circuit.

Moreover, if the resistor $R_1 \to \infty$ in Fig. 5(c), that is, R_1 is off, then $-R_1/R_2 \to -\infty$. The switching points $(E_i - V_{sat}R_2/R_1)$ and $(E_i + V_{sat}R_2/R_1)$ both tend to E_i. Therefore, the circuit to realize the SNLF tends to the SNFS. Equation (10) can be recasted as

$$U_o = \begin{cases} V_{sat} & if \quad U_i \le E_i, \\ -V_{sat} & if \quad U_i > E_i. \end{cases} \tag{12}$$

Similarly, the SNFS function $F_2(x)$ can be realized as follows:

$$f_2(u) = A_1 sgn(u) + \sum_{i=1}^{N} sgn(u - E_i) + \sum_{j=1}^{M} sgn(u + E_j),$$

where $E_i = 2iE_1$, $E_j = 2jE_2$, E_1 and E_2 are the unit voltages, and $E_1 = A_2$, $E_2 = A_3$. The circuit diagram is omitted here for the matter of saving space.

According to Min *et al.*,[40] the approximating fractional transfer function of order 0.96 is

$$H(s) = \frac{1.515(s + 1433)(s + 3.565)}{(s + 1821)(s + 4.532)(s + 0.01127)}.$$

The circuit to realize the 0.96 order differentiation is depicted in Fig. 6. The circuit values are calculated $R_3 = 81.95$ MΩ, $R_4 = 1.22$ MΩ, $R_5 = 0.0039$ MΩ, $C_1 = 0.232$ μF, $C_2 = 0.18$ μF, and $C_3 = 0.66$ μF, for $\alpha = 0.96$.

Based on all these rules, we choose the type 2 attractors as a vehicle to generate multi-directional MSCA of order 0.96, and a maximum 9×9 attractor is observed. The circuit diagram is represented in Fig. 7. This circuit diagram includes four different parts:

- Part 1: invert sum box N_0;
- Part 2: FO integrator box N_1;
- Part 3: invert box N_2;
- Part 4: saturated function generator SNLF.

Box F stands for the 0.96-order calculation unit shown in Fig. 6. Box SNLF stands for the saturated function unit in Fig. 5(c). All resistors marked $R_1 = 10$ kΩ, $R_2 = 100$ Ω. According to the Kirchhoff current law, and for the zero initial condition, we can derive the following equations:

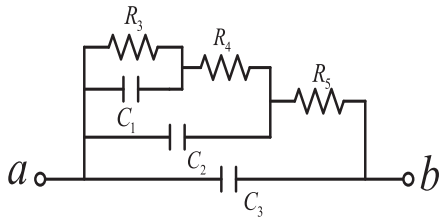

FIG. 6. Diagram of 0.96-order differential unit.

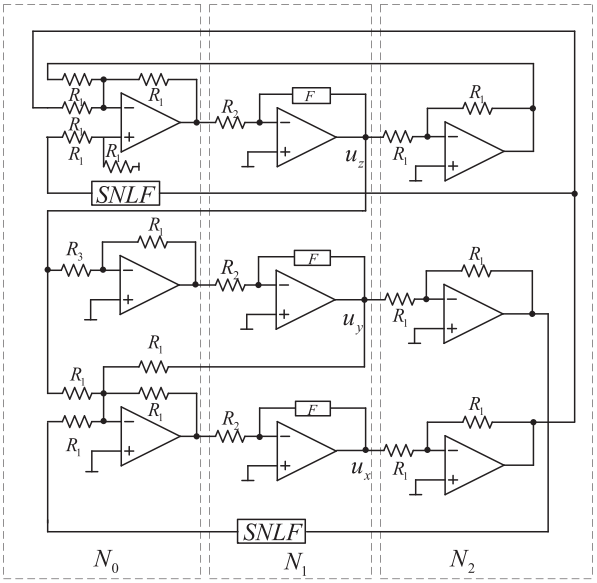

FIG. 7. Circuit diagram to generate attractors of type 2.

$$\begin{cases} R_2Cs^{0.96}U_x(s) = U_y(s) + U_z(s) - f\big(U_y(s)\big), \\ R_2Cs^{0.96}U_y = \dfrac{R_1}{R_2}U_z(s), \\ R_2Cs^{0.96}U_z(s) = -U_x(s) - U_z(s) + f(U_x(s)), \end{cases} \tag{13}$$

where $U_x(s)$, $U_y(s)$, $U_z(s)$, $f(U_x(s))$, $f(U_y(s))$ denote the Laplace transform of u_x, u_y, u_z, $f(u_x)$, $f(u_y)$, respectively. The expression $s^{0.96}$ denotes the 0.96-order Laplace transform. Equation (13) is equivalent to

$$\begin{cases} s^{0.96}U_x(s) = \dfrac{1}{R_2C}\big[U_y(s) + U_z(s) - f\big(U_y(s)\big)\big], \\ s^{0.96}U_y(s) = \dfrac{1}{R_2C}\dfrac{R_1}{R_3}U_z(s), \\ s^{0.96}U_z(s) = \dfrac{1}{R_2C}[-U_x(s) - U_z(s) + f(U_x(s))], \end{cases} \tag{14}$$

where $1/R_2C$ is the integrator constant of the circuit, and also the transformation factor of the time scale. The parameter $\mu = R_1/R_3$ is not unique, and in our system, we choose $\mu = 3$, yielding $R_3 = 3.3$ kΩ. The 9×9 attractors generated by SNLF in two directions are shown in Fig. 8(a). We can also observe other kinds of attractors by adjusting the circuit diagram. We list a few in Figs. 8(b)–8(d).

Remark 3. The primal FO linear systems used to generate MSCA are different from those in References 31–33 and 35–37.

Remark 4. It should be noted that most of the aforementioned MSCA were only verified by numerical simulations.[31–33,35–37] Here, circuit experiments have been carried out, which coincide with the theoretical results.

Remark 5. It follows from Table I and Fig. 1 that system (4) can also generate grid MSCA by employing one kind of function series(SNFS or SNLF). However, Topology structure of multi-directional MSCA generated by using SNLF and SNFS is different from ones by employing SNLF or SNFS; SNLF and SNFS belong to different kinds of

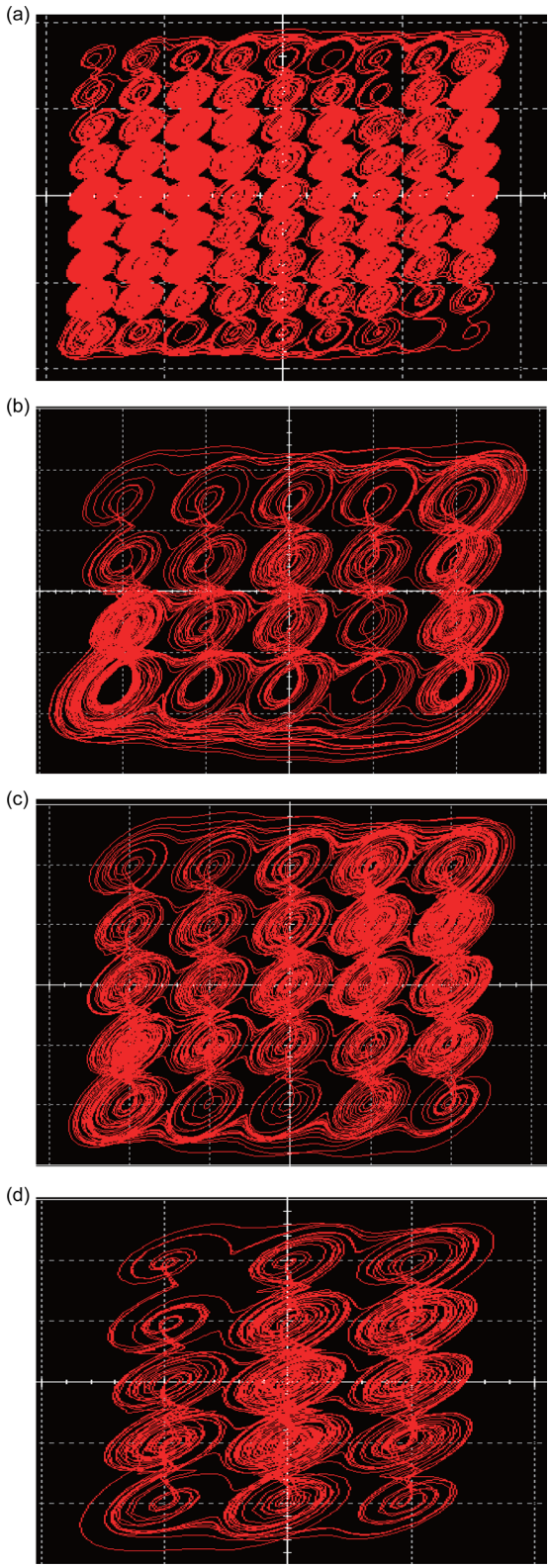

FIG. 8. Circuit results: (a) 9×9 attractors, where x-axis using SNLF, 5 V/div, y-axis using SNLF, 5 V/div; (b) 5×4 attractors, where x-axis using SNLF, 2 V/div, y-axis using SNLF, 2 V/div; (c) 5×5 attractors, where x-axis using SNLF, 2 V/div, y-axis using SNLF, 2 V/div; (d) 5×4 attractors, where x-axis using SNFS, 2 V/div, y-axis using SNFS, 2 V/div.

functions, which have different forming mechanisms. In addition, the complexity of the whole circuit is different because the ways of the circuit implementation of SNLF and SNFS are not same.

Remark 6. Here, to generate grid MSCA from FO linear system by using SNFS and SNLF can take advantage of their own strengths. It will increase even more flexibility to design MSCA at one's will. First, the distance between each scroll and size of each scroll can be designed by adjusting the parameters in SNFS, which also benefits circuit implementation. Second, since SNLF is more smooth than SNFS, widths, slopes, breakpoints, equilibrium points, and shapes of SNLF are adjustable easily, which offer more flexibility than SNFS.

V. CONCLUSION

A novel FO chaotic system is proposed and investigated in this paper. Multi-directional MSCA are created successfully by adding two different kinds of PWLF to a novel FO linear system. Chaotic behaviors of the system are verified by means of the stability of the equilibrium points, Lyapunov exponent, and Poincaré section. It is worth mentioning that for the first time the circuit implement of FO multi-directional multi-scroll chaotic system is discussed in this paper. Circuit implementation results confirm the theoretical analysis. Attractors of order 0.96 generated by four kinds of function combinations are observed.

ACKNOWLEDGMENTS

The authors would like to thank the anonymous referees and the editor for their valuable comments and suggestions. This work was supported by the National Natural Science Funds of China (Nos. 61403115, 11571016, and 51577046) and the Natural Science Foundation of Anhui Province (No. 1508085QF120) and the Fundamental Research Funds for the Central Universities (Nos. JZ2016HGTB0718 and JZ2016HGXJ0022).

[1]G. Chen and X. Dong, *From Chaos to Order: Methodologies, Perspectives and Applications* (World Scientific, Singapore, 1998).
[2]G. Chen and X. Yu, *Chaos Control: Theory and Applications* (Springer-Verlag, Heidelbert, Gemany, 2003).
[3]G. Chen and J. Lü, *Dynamics of the Lorenz Family: Analysis, Control, and Synchronization* (Science Press, Beijing, 2003).
[4]K. S. Tang, G. Q. Zhong, G. Chen, and K. F. Man, IEEE Trans. Circuits Syst. I: Fundam. Theory Appl. **48**, 1369 (2001).
[5]G. Zhong, K. F. Man, and G. Chen, Int. J. Bifurcation Chaos **12**, 2907 (2002).
[6]M. E. Yalcin, J. A. K. Suykens, J. Vandewalle, and S. Ozoguz, Int. J. Bifurcation Chaos **12**, 23 (2002).
[7]J. Lü, X. Yu, and G. Chen, Proc. Phys. Control **2**, 420 (2003).
[8]J. Lü, J. Syst. Sci. Complexity **16**, 404 (2003).
[9]F. Han, X. Yu, Y. Wang, Y. Feng, and G. Chen, Electron. Lett. **39**, 1636 (2003).
[10]J. Lü, F. Han, X. Yu, and G. Chen, Automatica **40**, 1677 (2004).
[11]F. Han, J. Lü, X. Yu, G. Chen, and Y. Feng, Dyn. Contin. Discrete Impulse Syst. Ser. B **12**, 95 (2005).
[12]J. Lü, G. Chen, X. Yu, and H. Leung, IEEE Trans. Circuits Syst. I: Fundam. Theory Appl. **51**, 2476 (2004).
[13]C. X. Zhang and S. M. Yu, Acta Phys. Sin. **58**, 120 (2009).
[14]T. Zuo, K. H. Sun, X. X. Ai, and H. H. Wang, IEEE Trans. Circuits Syst. II **61**, 818 (2014).
[15]X. M. Wu and Y. G. He, Int. J. Bifurcation Chaos **25**, 1550041 (2015).
[16]Z. Elhadj and J. C. Sprott, Int. J. Bifurcation Chaos **23**, 1350120 (2013).
[17]K. B. Oldhamm and J. Spanier, *The Fractional Calculus* (Academic Press, New York, 1974).
[18]S. M. Kenneth and R. Bertram, *An Introduction to Fractional Calculus and Fractional Differential Equations* (Wiley-Interscience, USA, 1993).

[19]I. Podlubny, *Fractional Differential Equations* (Academic Press, New York, 1999).
[20]P. L. Butzer and U. Westphal, *An Introduction to Fractional Calculus* (World Scientific, Singapore, 2000).
[21]C. P. Li, F. R. Zhang, J. Kurths, and F. H. Zeng, Philos. Trans. R. Soc. London, Ser. A **371**, 20120155 (2013).
[22]F. R. Zhang, G. R. Chen, C. P. Li, and J. Kurths, Philos. Trans. R. Soc. London, Ser. A **371**, 20120156 (2013).
[23]C. P. Li, Y. Q. Chen, and J. Kurths, Philos. Trans. R. Soc. London, Ser. A **371**, 20130037 (2013).
[24]X. Gao and J. Yu, Chaos, Solitons Fractals **24**, 1097 (2005).
[25]D. Cafagna and G. Grassi, Int. J. Bifurcation Chaos **18**, 615 (2008).
[26]C. Li and G. Chen, Physica A **341**, 55 (2004).
[27]C. P. Li and G. J. Peng, Chaos, Solitons Fractals **22**, 443 (2004).
[28]I. Grigorenko and E. Grigorenko, Phys. Rev. Lett. **91**, 034101 (2003).
[29]G. J. Lü, Phys. Lett. A **354**, 305 (2006).
[30]X. Y. Wang and M. J. Wang, Chaos **17**, 033106 (2007).
[31]W. H. Deng and J. Lü, Chaos **16**, 043120 (2006).
[32]W. H. Deng, Int. J. Bifurcation Chaos **17**, 3965 (2007).
[33]W. H. Deng and J. H. Lü, Phys. Lett. A **369**, 438 (2007).
[34]D. Cafagna and G. Grass, Nonlinear Dyn. **70**, 1185 (2012).
[35]G. Sun, M. Wang, L. Huang, and L. Shen, Circuits Syst. Signal Process. **30**, 1183 (2011).
[36]W. Ahmad, Chaos, Solitons Fractals **25**, 727 (2005).
[37]F. Xu, Int. J. Bifurcation Chaos **24**, 1450029 (2014).
[38]C. P. Li and Y. T. Ma, Nonlinear Dyn. **71**, 621 (2013).
[39]P. S. Christopher, IEEE Trans. Circuits Syst. I: Fundam. Theory Appl. **4**, 675 (1993).
[40]F. H. Min, S. Y. Shao, W. D. Huang, and E. R. Wang, Chin. Phys. Lett. **32**, 030503 (2015).